Available online at www.sciencedirect.com
ScienceDirect
Journal of Organometallic Chemistry 692 (2007) 5285–5294
Journal of Organometallic Chemistry
www.elsevier.com/locate/jorganchem

Palladium(II)/allylpalladium(II) complexes with xanthate ligands: Single-source precursors for the generation of palladium sulfide nanocrystals

Anshu Singhal [a,*], Dimple P. Dutta [a], Avesh K. Tyagi [a], Shaikh M. Mobin [b], Pradeep Mathur [b,c], Ingo Lieberwirth [d]

[a] Chemistry Division, Bhabha Atomic Research Centre, Trombay, Mumbai 400 085, India
[b] National Single-Crystal X-ray Diffractometer Facility, Indian Institute of Technology, Powai, Mumbai 400 076, India
[c] Department of Chemistry, Indian Institute of Technology, Powai, Mumbai 400 076, India
[d] Max Planck Institute for Polymer Research, Ackermannweg 10, D-55128 Mainz, Germany

Received 19 June 2007; received in revised form 1 August 2007; accepted 10 August 2007
Available online 17 August 2007

Abstract

In an effort to find simple and common single-source precursors for palladium sulfide nanostructures, palladium(II) complexes, $[Pd(S_2X)_2]$ (X = COMe (**1**), CO^{i}Pr (**2**)) and η^3-allylpalladium complexes with xanthate ligands, $[(\eta^3\text{-}CH_2C(CH_3)CR_2)Pd(S_2X)]$ (R = H, X = COMe (**3**); R = H, X = COEt (**4**); R = H, X = CO^{i}Pr (**5**); R = CH_3, X = COMe (**6**)), have been investigated. The crystal structures of $[Pd(S_2X)_2]$ (X = COMe (**1**), Co^{i}Pr (**2**)) and $[(\eta^3\text{-}CH_2C(CH_3)CH_2)Pd(S_2COMe)]$ (**3**) have been established by single crystal X-ray diffraction analysis. The complexes, **1**, **2** and **3** all contain a square planar palladium(II) centre. In the allyl complex **3**, this is defined by the two sulfurs of the xanthate and the outer carbons of the 2-methylallyl ligand, while in the complexes, **1** and **2** it is defined by the four sulfur atoms of the xanthate ligand. Thermogravimetric studies have been carried out to evaluate the thermal stability of η^3-allylpalladium(II) analogues. The complexes are useful precursors for the growth of nanocrystals of PdS either by furnace decomposition or solvothermolysis in dioctyl ether. The solvothermal decomposition of complexes in dioctyl ether gives a new metastable phase of PdS which can be transformed to the more stable tetragonal phase at 320 °C. The nanocrystals obtained have been characterized by PXRD, SEM, TEM and EDX.

Keywords: η^3-Allylpalladium complexes; Xanthate ligands; X-ray; Thermogravimetric studies; Transmission electron microscopy

1. Introduction

Platinum group metal chalcogenides find extensive applications in catalysis [1–5] and material science [6–8]. PdS, a semiconducting sulfide ($E_g = \sim 2.0$ eV), in particular, can be used as a catalyst for dehydrogenation [9] and dehydrodesulfurisation [10] of several thiophene derivatives. It has also been employed as light image receiving material with silver halides [11], for lithographic films [12] and lithographic plates with high resolution [13]. Given the use and potential applications of PdS, the challenge is to generate high quality PdS in both an economical and reliable fashion. In earlier studies, semiconducting films of palladium sulfide polymer composite have been obtained when organosols of PdS in DMF were prepared by the reaction of the metal acetate with hydrogen sulfide, followed by addition of polymers [14]. Aqueous dispersions of PdS particles have been prepared from $PdCl_2$ or Na_2PdCl_4 with Na_2S solutions [15]. Uniform spherical particles with mean diameter 20–30 nm have been obtained in acidic medium in the presence or absence of surfactants.

There have been several reports recently on the use of single-source precursors, containing both palladium and sulfur within the one molecule, for the growth of PdS

* Corresponding author. Tel.: +91 22 255590281; fax: +91 22 25505151.
E-mail address: ansing@barc.gov.in (A. Singhal).

0022-328X/$ - see front matter © 2007 Elsevier B.V. All rights reserved.
doi:10.1016/j.jorganchem.2007.08.015

nanostructures either by solvothermal process or by CVD methods. The major advantages of the single-source approach over conventional MOCVD using dual sources, include limited pre-reactions and good quality films. Palladium compounds that have been investigated recently in this context include bis(*O*-isopropyldithiocarbonato)palladium(II) [16] i.e., $[Pd(S_2CO^iPr)_2]$ and bis(*n*-hexyl(methyl)-dithiocarbamato)palladium(II) [17] i.e. $[Pd(S_2CNMeHex)_2]$. Very recently, Hogarth et al. have reported preparation of nonstoichiometric palladium sulfide films ($Pd_{2.8}S$) from allylpalladium dithiocarbamate precursor, $[\eta^3\text{-}(C_3H_5)Pd\text{-}(S_2CNMeHex)]$ [18]. We have earlier reported the synthesis of metal rich palladium sulfide (Pd_4S) from organosulfur-bridged dimeric 2-methylallylpalladium complexes [19]. The palladium sulfide was obtained by furnace decomposition and refluxing the complexes in xylene.

Xanthate ligands $[RCOS_2]^-$ are known to coordinate metal centers in a variety of coordination modes, e.g. monodentate, bidentate chelating or bridging [20]. The ligands can be easily prepared and their properties can be suitably modified by appropriate choice of the O bound substituents. Further, the metal xanthate complexes show interesting thermal behaviour and thermal decomposition of such complexes can be a useful route to metal sulfides [21]. Recently, metal alkylxanthate compounds have been used as synthetic precursors for generation of metal sulfide nanostructures [22–24]. In view of this, we decided to explore the suitability of palladium and η^3-allylpalladium complexes as single-source precursors for the preparation of nanocrystalline palladium sulfide.

The synthesis of xanthate complexes of palladium (**1** and **2**) [25] and 2-methylallylpalladium (**3** and **4**) [26] has been reported in the literature. Till date, the single-crystal X-ray structures of only one binary alkylxanthate of palladium(II), $[Pd(S_2COEt)_2]$ [27] is reported. The other X-ray structures reported are for the complexes $[Pd(S_2COCH_2CF_3)_2]$ [28], and $[Pd(S_2COC_6H_2\text{-}2,4,6\text{-}Me_3)_2]$ [29]. In this study, we report for the first time, thermogravimetric studies on η^3-allylpalladium(II) complexes with xanthate ligands and their application for the generation of PdS nanocrystals by furnace and solvothermal decomposition. We also report an alternate and convenient method of synthesis of the complexes **1** and **2**, NMR characterization data for the known and new complexes and the single crystal X-ray structures of $[Pd(S_2COMe)_2]$ (**1**) and $[Pd(S_2CO^iPr)_2]$ (**2**) and $[(\eta^3\text{-}CH_2C(CH_3)CH_2)Pd\text{-}(S_2CO\text{-}Me)]$ (**3**). Our report on the single crystal X-ray structure of complex **3** is the first ever report on structural investigation of any allylpalladium complex with xanthate ligand to the best of our knowledge.

2. Results and discussion

2.1. Synthesis and characterization of the complexes

The mononuclear complexes, $[Pd(S_2X)_2]$ (X = COMe, CO^iPr) and $[(\eta^3\text{-}CH_2C(CH_3)CR_2)Pd(S_2X)]$ (R = H or CH_3; X = COMe, COEt, CO^iPr) have been prepared by reacting either $[PdCl_2(MeCN)_2]$ or $[(\eta^3\text{-}CH_2C(CH_3)CR_2)\text{-}Pd(\mu\text{-}Cl)]_2$ with anhydrous sodium/potassium salts of xanthates in 1:2 stoichiometry in acetonitrile solution at room temperature for 0.5 h. The syntheses are straightforward and all the complexes can be prepared in good yields. The earlier method reported for preparation of **1** and **2** involves the reaction between $PdCl_2$ and potassium alkyl xanthates in aqueous solution and the complexes obtained need to be dried in vacuo for several days and subsequently sublimed in order to obtain pure products [25]. By following our method we could get pure product by simple recrystallization from CH_2Cl_2–hexane mixture. In the complexes, **3–6** the sulfur donor ligands are bidentate, forming Pd–S–C–S palladacycles with η^3-allyl group completing the coordination sphere.

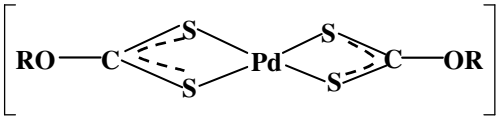

R=Me(**1**); R=^{i}Pr (**2**)

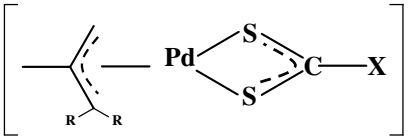

R = H, X = COMe (**3**); R = H, X = COEt (**4**); R = H, X = CO^iPr (**5**); R = CH_3, X = COMe (**6**).

All the complexes are yellow or orange solids readily soluble in most of the common organic solvents and can be stored at 0 °C for long periods without any decomposition.

Assignments of IR spectra are made by reference to literature data on related complexes [30]. IR spectra of complexes, **3–6** exhibit bands characteristic of a bidentate dithiocarbonate ligand in the range 1240–1250 cm^{-1}, this being attributed to ν(C–O), while strong band at 1028–1032 cm^{-1} results from ν(C–S) vibration.

The ^1H NMR spectra of the complexes, $[(\eta^3\text{-}CH_2\text{-}C(CH_3)CH_2)Pd(S_2X)]$ are straightforward showing correct proton ratios and peak multiplicities for both the allyl and xanthate ligands. In such complexes, singlets for each methyl group, *syn* and *anti* protons are observed. Similarly, all the expected peaks could be seen in the carbon-13 NMR spectra (see Section 4).

2.2. X-ray crystal structure

The molecular structures of $[(PdS_2COMe)_2]$ (**1**) and $[Pd(S_2CO^iPr)_2]$ (**2**) and $[(\eta^3\text{-}CH_2C(CH_3)CH_2)Pd(S_2COMe)]$ (**3**) as shown in Figs. 1–3, respectively, have been estab-

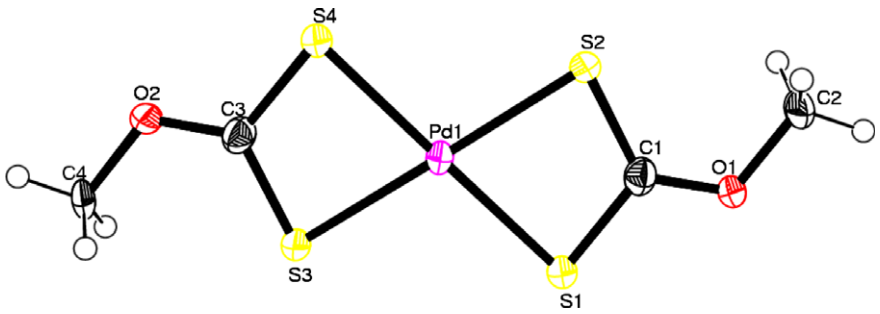

Fig. 1. The molecular structure of complex **1** showing atomic numbering scheme.

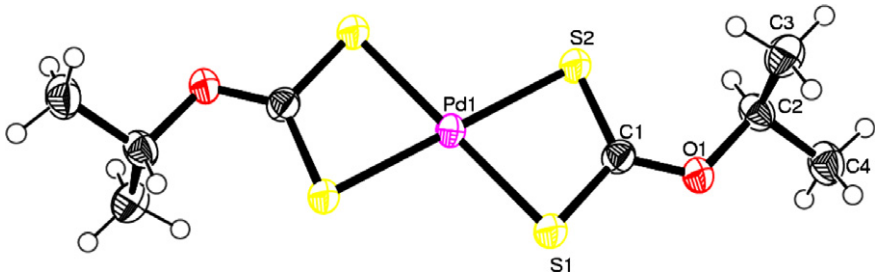

Fig. 2. The molecular structure of complex **2** showing atomic numbering scheme.

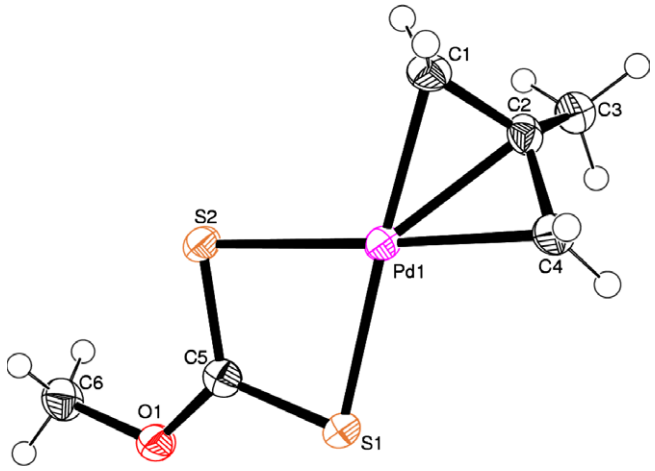

Fig. 3. The molecular structure of complex **3** showing atomic numbering scheme.

Table 1
Selected geometric parameters (Å, °) for complex **1**

Pd(1)–S(4)	2.322(2)	S(4)–Pd(1)–S(1)	177.88(5)
Pd(1)–S(1)	2.334(2)	S(4)–Pd(1)–S(3)	75.53(6)
Pd(1)–S(3)	2.336(2)	S(1)–Pd(1)–S(3)	104.60(6)
Pd(1)–S(2)	2.340(2)	S(4)–Pd(1)–S(2)	104.15(5)
S(1)–C(1)	1.706(7)	S(1)–Pd(1)–S(2)	75.60(6)
S(2)–C(1)	1.704(7)	S(3)–Pd(1)–S(2)	176.94(5)
S(3)–C(3)	1.706(6)	C(1)–S(1)–Pd(1)	85.1(2)
S(4)–C(3)	1.698(6)	C(1)–S(2)–Pd(1)	85.0(2)
O(1)–C(1)	1.293(8)	C(3)–S(3)–Pd(1)	85.0(2)
O(1)–C(2)	1.458(7)	C(3)–S(4)–Pd(1)	85.6(2)
O(2)–C(3)	1.296(8)	C(1)–O(1)–C(2)	118.8(5)
O(2)–C(4)	1.442(7)	C(3)–O(2)–C(4)	118.5(5)
		O(1)–C(1)–S(2)	126.9(5)
		O(1)–C(1)–S(1)	118.8(5)
		S(2)–C(1)–S(1)	114.3(4)

lished unambiguously by single crystal X-ray diffraction analyses. Selected bond lengths and bond angles for complexes **1**, **2** and **3** are given in Tables 1–3, respectively. In the bis(xanthate) complex **1**, palladium(II) adopts a slightly distorted square planar geometry within an almost symmetric S_4 donor set, the Pd–S distances are not significantly different and the S–C, C–O, and O–C distances have usual lengths (Table 1). The structure of $[Pd(S_2CO^iPr)_2]$, with Pd–S distances of 2.317(2) and 2.326(2) Å in the centrosymmetric and square-planar molecule, is isomorphous with $[Pd(S_2COEt)_2]$ [27]. The intraligand S(1)–Pd–S(2) angles of 75.60(6)° and 75.24(8)° for complexes **1** and **2**, respectively, indicate considerable strain within the four-membered 1,1-dithiolato-chelate.

Table 2
Selected geometric parameters (Å, °) for complex **2**

Pd(1)–S(1)#1	2.317(2)	S(1)#1–Pd(1)–S(1)	180.00(5)
Pd(1)–S(1)	2.317(2)	S(1)#1–Pd(1)–S(2)	104.76(8)
Pd(1)–S(2)	2.326(2)	S(1)–Pd(1)–S(2)	75.24(8)
Pd(1)–S(2)#1	2.326(2)	S(1)#1–Pd(1)–S(2)#1	75.24(8)
S(1)–C(1)	1.679(9)	S(1)–Pd(1)–S(2)#1	104.76(8)
S(2)–C(1)	1.690(9)	S(2)–Pd(1)–S(2)#1	180.00(13)
O(1)–C(1)	1.317(11)	C(1)–S(1)–Pd(1)	85.3(3)
O(1)–C(2)	1.477(10)	C(1)–S(2)–Pd(1)	84.8(3)
		C(1)–O(1)–C(2)	119.2(7)
		O(1)–C(1)–S(1)	118.5(6)
		O(1)–C(1)–S(2)	126.9(7)
		S(1)–C(1)–S(2)	114.6(5)

Symmetry transformations used to generate equivalent atoms: #1 $-x$, $-y$, $-z$.

Table 3
Selected geometric parameters (Å, °) for complex **3**

Pd(1)–C(2)	2.133(3)	C(2)–Pd(1)–C(4)	38.66(12)
Pd(1)–C(4)	2.137(3)	C(2)–Pd(1)–C(1)	38.37(11)
Pd(1)–C(1)	2.138(3)	C(4)–Pd(1)–C(1)	68.07(12)
Pd(1)–S(1)	2.375(2)	C(2)–Pd(1)–S(1)	139.68(8)
Pd(1)–S(2)	2.384(2)	C(4)–Pd(1)–S(1)	107.83(9)
S(1)–C(5)	1.697(3)	C(1)–Pd(1)–S(1)	174.78(9)
S(2)–C(5)	1.697(3)	C(2)–Pd(1)–S(2)	140.13(9)
O(1)–C(5)	1.319(4)	C(4)–Pd(1)–S(2)	175.95(9)
O(1)–C(6)	1.450(4)	C(1)–Pd(1)–S(2)	108.95(9)
C(1)–C(2)	1.403(4)	S(1)–Pd(1)–S(2)	74.97(3)
C(2)–C(4)	1.414(4)	C(5)–S(1)–Pd(1)	84.03(11)
C(2)–C(3)	1.508(5)	C(5)–S(2)–Pd(1)	83.75(11)
		C(5)–O(1)–C(6)	118.4(2)
		C(2)–C(1)–Pd(1)	70.63(17)
		C(1)–C(2)–C(4)	116.3(3)
		C(1)–C(2)–C(3)	121.1(3)
		C(4)–C(2)–C(3)	121.4(3)
		C(1)–C(2)–Pd(1)	71.00(18)
		C(4)–C(2)–Pd(1)	70.85(18)
		C(3)–C(2)–Pd(1)	117.7(2)
		O(1)–C(5)–S(2)	124.7(2)
		O(1)–C(5)–S(1)	118.1(2)
		S(2)–C(5)–S(1)	117.2(2)

In case of 2-methylallyl palladium(II) complex **3**, the central allyl carbon atom C(2) and O(1) atom of dithiocarbonate, lie on the same side of the coordination plane defined by S(1)–Pd(1)–S(2). The geometric parameters fall in the expected ranges as observed for other allylpalladium complexes [19,31,32]. The coordination geometry around the metal centre is distorted square planar with the S(1)–Pd(1)–S(2) and C(1)–Pd(1)–C(4) bond angles at 74.97(3)° and 68.07°, respectively. The two terminal allyl carbon atoms are not exactly coplanar with the coordination plane formed by S(1)–Pd(1)–S(2). The terminal Pd–C(allyl) bond lengths are almost similar whereas the bond length of Pd–C(2) is shorter. The S atom in xanthate ligands is a weak donor atom but can interact with acceptors to help define the crystal packing of the molecules. A view of the extended chain propagated along the crystallographic *a*-direction is shown in Fig. 4 for complex **3**. The H atom of 2-methylallyl CH_2 group forms intermolecular interaction with sulfur atom of other molecule forming a linear chain along *a*-axis. The S···H bond distance is found to be 2.956 Å.

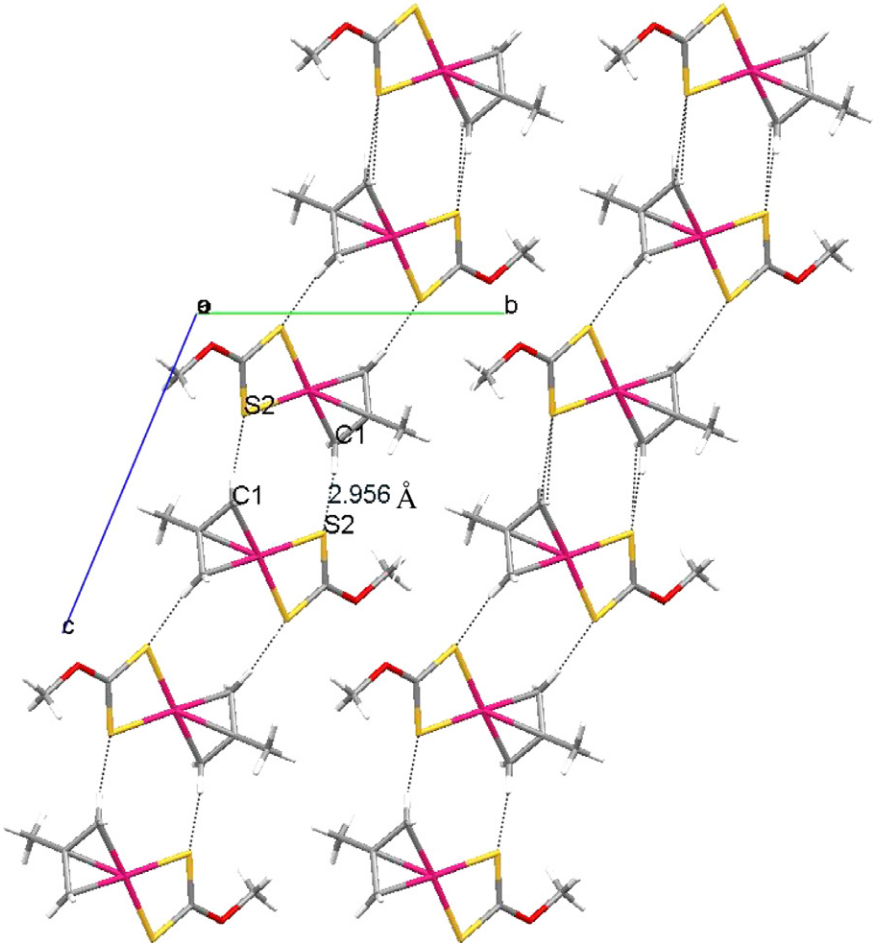

Fig. 4. Packing diagram for complex **3** showing S···H interaction.

2.3. Thermogravimetric studies

To evaluate the thermal stability of each complex in a quantitative manner, thermogravimetric studies on $[(\eta^3\text{-}CH_2C(CH_3)CR_2)Pd(S_2X)]$ have been carried out in flowing nitrogen atmosphere. Fig. 5 shows the thermogram for each complex. The TG studies indicate that these complexes thermally decompose in two/three superimposible steps to leave a residue of palladium sulfide. Because of the superimposing nature of the decomposition steps, the mechanism of thermal decomposition of these complexes could not be worked out unambiguously. However, the total mass loss obtained from TGA in all the complexes agrees well within experimental error with the calculated mass loss for the formation of PdS. As shown by TG traces, the complexes **3**–**6** decompose at 90, 101, 111 and 116 °C, respectively.

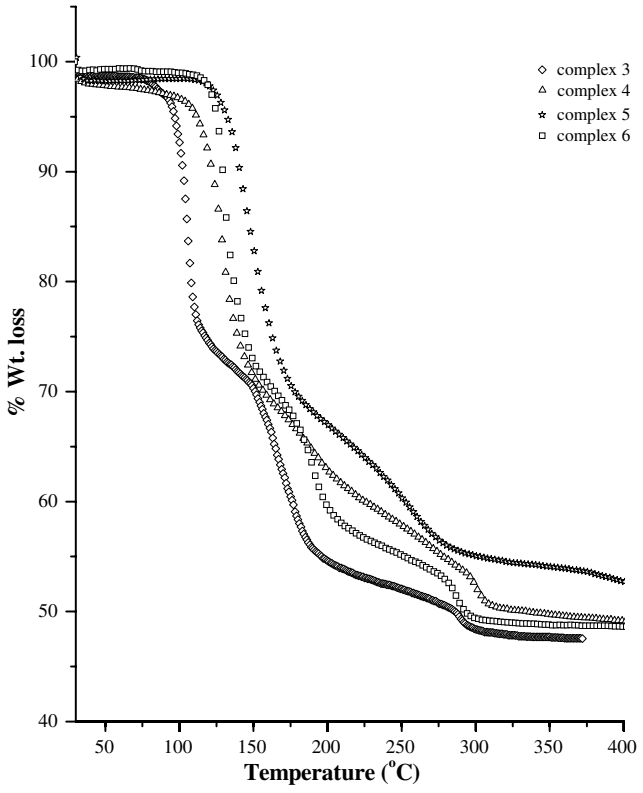

Fig. 5. TG traces for the complexes $[(\eta^3\text{-}CH_2C(CH_3)CR_2)Pd(S_2COR)]$. XRD analyses of residues revealed them to be PdS.

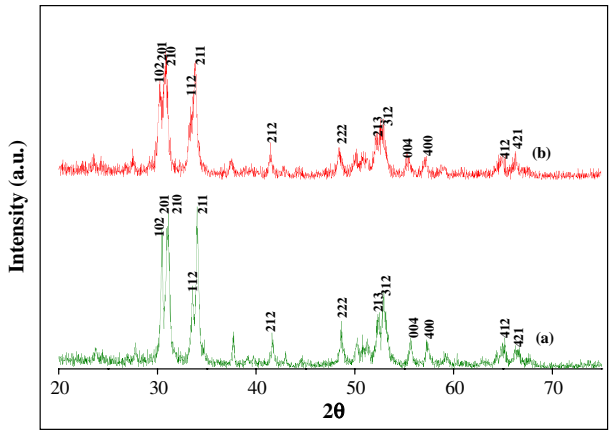

Fig. 6. X-ray diffraction patterns for the products obtained after thermolysis of complex **1** (a) and **3** (b) in furnace at 300 °C.

2.4. Thermolysis of $\{Pd(S_2COMe)_2]$ (**1**) and $[(\eta^3\text{-}CH_2C(CH_3)CH_2)Pd(S_2COMe)]$ (**3**)

Thermal decomposition of the above complexes has been carried out at 300 °C at a rate of 5 °C min^{-1} in a furnace under an argon atmosphere. X-ray diffraction pattern of the products obtained compare well with the pattern reported for palladium sulfide [33] and could be assigned to the tetragonal phase of the PdS. Fig. 6a and b show XRD patterns of the products obtained from thermolysis of **1** and **3**, respectively. The average crystallite sizes of 32 nm and 16 nm are estimated with the Scherrer equation for the particles obtained from complexes **1** and **3**, respectively, after applying correction due to instrumental line broadening. The surface morphology of the particles obtained from thermolysis of complex **3** has been studied by scanning electron microscopy. The scanning electron micrographs taken at different resolutions show spherical aggregates of micro crystals (Fig. 7) The chemical composition of the products has been verified by energy dispersive X-ray spectroscopy (Expected atom % Pd: 50; S: 50%: observed Pd: 50.19; S: 49.81%; {decomposed product from complex **1**} Pd: 50.28; S: 49.72% {decomposed product from complex **3**}), which is in very close agreement with the nominal composition PdS.

2.5. Thermal decomposition of complexes $[(\eta^3\text{-}CH_2C(CH_3)CH_2)Pd(S_2X)]$ (X = COMe; COEt; CO^iPr) in dioctyl ether

Thermal decomposition of complexes, $[(\eta^3\text{-}CH_2\text{-}C(CH_3)CH_2)Pd(S_2X)]$ has been carried out in dioctyl ether at 260 °C. The X-ray diffraction patterns of the products obtained are shown in the Fig. 8. In the beginning, the patterns obtained could not be identified to any of the known phases. To know exactly what product we have got, the product obtained from solvothermolysis of complex **3** was annealed at 300 °C for 12 h after sealing the sample under vacuum. The X-ray diffraction pattern of the annealed sample could be assigned to tetragonal phase of the PdS [33] (Fig. 8d). This led us to believe that we may have obtained a new metastable crystallographic phase of PdS after thermal decomposition of complexes at 260 °C. To corroborate this fact, we have carried out DSC, TG-DTA studies and high temperature XRD study under vacuum on the same product. While in TG studies, practically no weight loss was observed while heating the sample from room temperature to 400 °C, in DSC a sharp exotherm can be observed at 323 °C (Fig. 9) further strengthening our

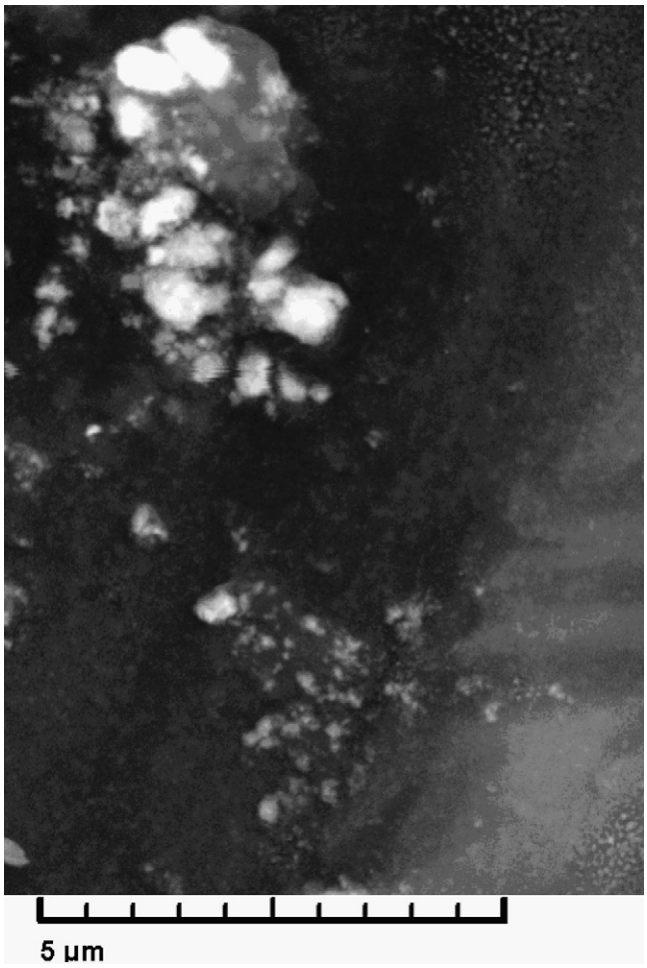

Fig. 7. Scanning electron micrograph of PdS nanocrystals obtained from thermolysis of complex **3** in furnace at 300 °C.

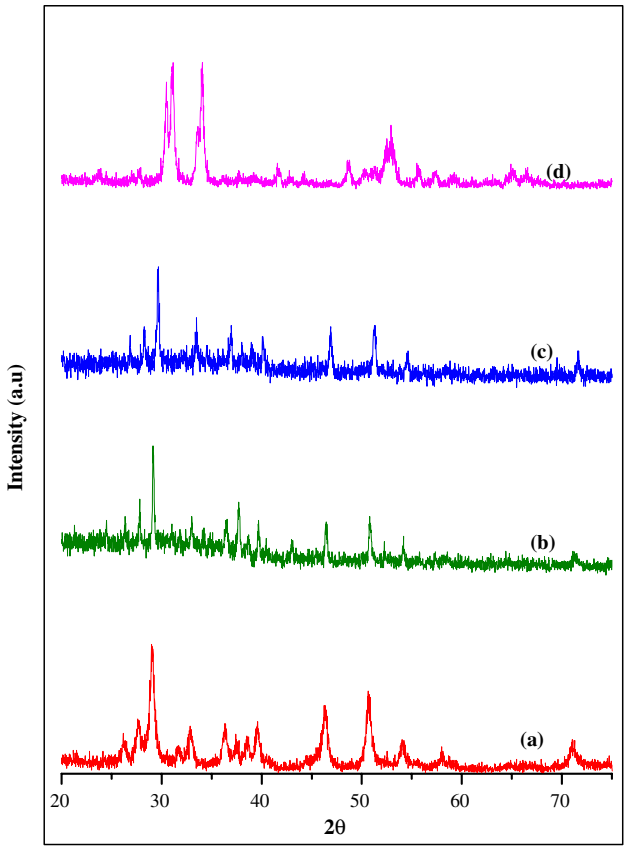

Fig. 8. X-ray diffraction patterns obtained after solvothermolysis of complexes, **3** (a); **4** (b), **5** (c) in dioctyl ether and for the annealed sample from the thermolysis product from complex, **3** (d).

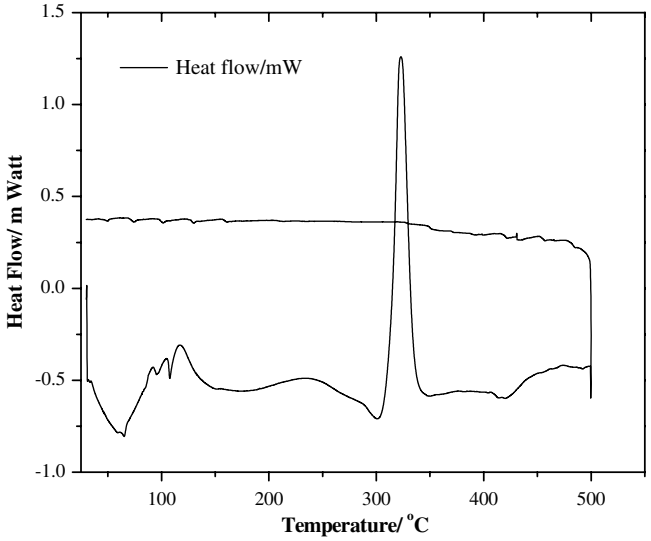

Fig. 9. Differential scanning thermogram for the PdS nanocrystals obtained from thermolysis of complex **3** in dioctyl ether. The peak at 100 °C is because of moisture evaporation.

belief that there exists a metastable phase of PdS. However, no endotherm was observed in differential scanning thermogram while cooling the sample at the same rate indicating the irreversible nature of the transition. DSC results clearly indicate that there is no chemical change in the product when heated from room temperature to 400 °C. High temperature X-ray diffraction patterns obtained by carrying out the study in the temperature range 30–400 °C at an interval of 50 °C are shown in Fig. 10. From the figure, one can clearly see that the room temperature phase is maintained up to 300 °C. At 350 °C, the peaks due to room temperature phase start diminishing irreversibly and peaks due to tetragonal phase of PdS start appearing. At 400 °C the phase is essentially tetragonal.

We have further, tried to index the powder XRD data obtained for the metastable phase of PdS nanocrystals using the program 'POWDERX' [34]. The data could be indexed on a monoclinic unit cell. All the peaks could be indexed (Table 4). Subsequently, the indexed data has been satisfactorily refined using the same program by least square refinement. However, it may be added that the indexing and refining of the obtained metastable phase of PdS further needs to be confirmed using a suitable structural model, which is not the main focus of the present investigation and hence will be done afterwards.

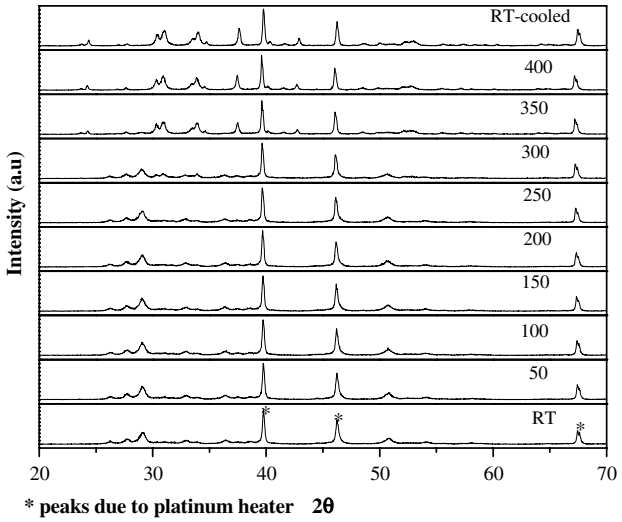

Fig. 10. High-temperature X-ray diffraction patterns obtained after heating PdS nanocrystals obtained from complex **3** indicating formation of tetragonal phase of PdS at 350 °C.

Table 4
Indexed powder X-ray data for the metastable phase of PdS nanocrystals obtained from complex **3**

d_{obs} (Å)	d_{calc} (Å)	h	k	l	Intensity (%)
3.3900	3.3898	2	0	0	25.7
3.2175	3.2175	−2	0	1	43.3
3.0656	3.0654	2	1	0	100.0
2.7245	2.7268	−1	0	2	37.3
2.4667	2.4648	2	2	0	39.7
2.3957	2.3962	−2	2	1	24.7
2.3311	2.3305	1	0	2	32.7
2.2747	2.2764	−3	0	1	38.3
1.9586	1.9553	2	3	0	56.9
1.7975	1.7976	0	0	3	61.2
1.6957	1.6949	4	0	0	27.7
1.3232	1.3224	2	5	0	28.6

Refined cell parameters: $a = 6.961(2)$ Å; $b = 7.188(2)$ Å; $c = 5.534(2)$ Å; $\beta = 103.41°$; volume = 269.8(1) Å^3

The surface morphology of the nanocrystals has been explored by TEM measurements and chemical composition by in situ TEM–EDX measurements. Fig. 11 shows the TEM image of the nanocrystals obtained by solvothermolysis of [(η^3-$CH_2C(CH_3)CH_2$)Pd(S_2COMe)] (**3**) in dioctyl ether at 260 °C. The particles are nearly spherical in shape and polydisperse, having average mean diameters in the range 8–20 nm. Fig. 12 shows the selected area diffraction pattern (SAED) of the particles confirming formation of nanocrystalline PdS. The chemical composition of the nanocrystals has been verified by in situ TEM–EDX analysis. The EDX analysis of PdS nanocrystals collected at two different locations on the solvothermolysis product from complex **3** is shown in Table 5. The results are in close agreement with the expected values (expected wt % for PdS: Pd, 76.84; S, 23.15%).

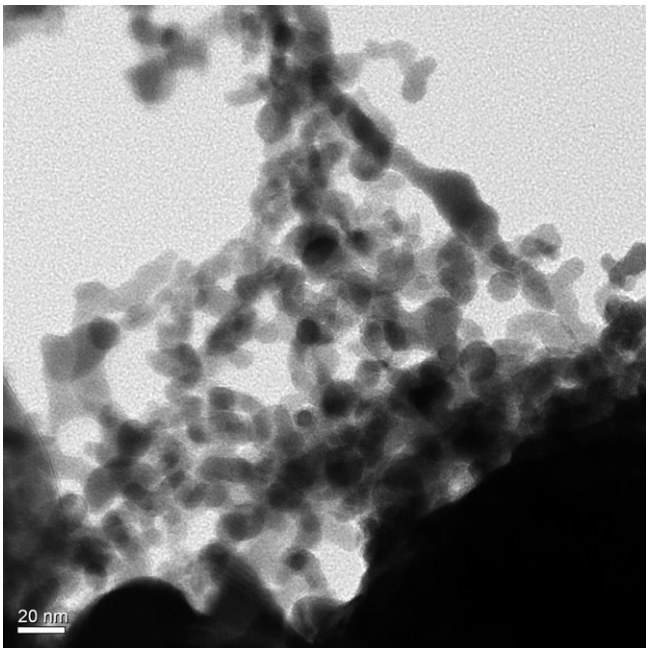

Fig. 11. Transmission electron micrograph of PdS nanocrystals (metastable phase) obtained from solvothermolysis of complex **3** in dioctyl ether.

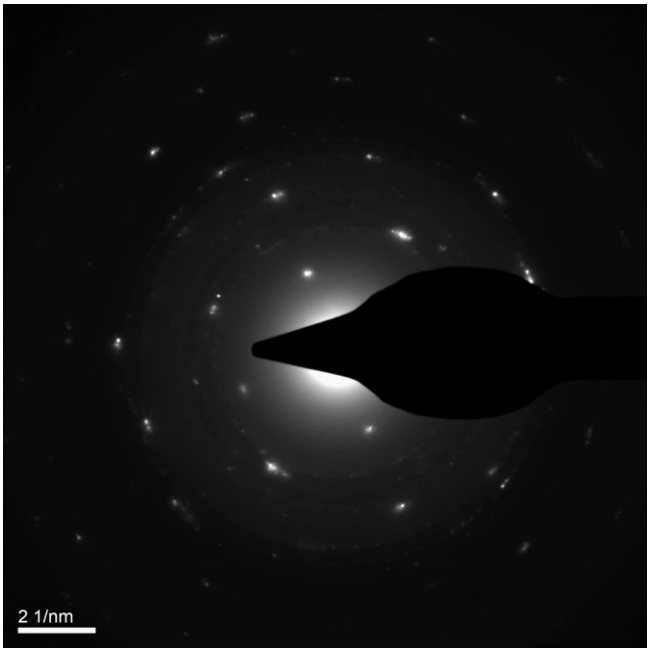

Fig. 12. SAED pattern obtained for metastable phase of PdS nanocrystals obtained from thermolysis of complex **3** in dioctyl ether.

Table 5
EDX data for PdS nanocrystals obtained from solvothermolysis of complex **3** in dioctyl ether at 260 °C

Element	Weight %	Weight %
S	23.81	21.62
Pd	76.19	78.38

It will be worth mentioning here, that solvothermal decomposition of the complexes **1**–**6** in TOPO at 260 °C for 1 h gave amorphous products as no diffraction pattern upon X-ray diffraction analysis could be observed. EDX analyses on the products showed them to be PdS.

3. Conclusions

Palladium(II) and η^3-allylpalladium(II) complexes with xanthate ligands have been prepared by following a facile synthetic approach and structurally characterized. The complexes have proven to be useful as single-source precursors for the generation of PdS nanocrystals by either furnace decomposition or solvothermal decomposition in dioctyl ether.

4. Experimental

4.1. General remarks

All the reactions were carried out under an atmosphere of dry argon using standard Schlenk techniques. Solvents were distilled from the appropriate drying agents and degassed before use. The chloro-bridged allylpalladium dimers, $[(\eta^3\text{-}CH_2C(CH_3)CR_2)Pd(\mu\text{-}Cl)]_2$ [35] and Na/KS_2COR [36] were prepared by following literature procedures. Melting points were determined in sealed capillaries with an electro thermal melting point apparatus and are uncorrected. C, H, N analyses were carried out with a Thermo Finnigan Flash 1112 series elemental analyser. Infrared spectra were recorded in the range 4000–200 cm^{-1} on a Bomem MB-102 FT-IR spectrophotometer as Nujol mulls between polythene sheets. ^1H and $^{13}C\{^1H\}$ spectra were recorded on a Bruker DPX 300 spectrometer operating at 300 and 75 MHz, respectively. Chemical shifts are referenced to the internal chloroform peak. Thermogravimetric analyses (TGA) were carried out using NETZSCH STA 409 PC/PG instrument. The TG curves were recorded at a heating rate of 5 °C min^{-1} under a flow of nitrogen gas. DSC measurements were performed on a Mettler Toledo instrument (Model DSC 823^e). DSC thermogram was recorded at a heating rate of 5 °C min^{-1} under a flow of nitrogen gas and cooling rate was also 5 °C min^{-1}. X-ray powder diffraction data were collected on a Philips X-ray diffractometer (Model PW 1729) using Cu K_α radiation (λ 1.54060 Å) at 30 kV and 20 mA. High Temperature XRD data was collected on a Philips X'Pert Pro XRD unit equipped with Anton Paar HTK attachment. All the measurements were performed under vacuum. SEM micrographs of the samples were obtained using a Vega MV2300t/40 scanning electron microscope. The chemical composition of the nanocrystals obtained from furnace decomposition of the precursors was examined by using a Inca Energy 250 instrument coupled to Vega MV2300t/40 scanning electron microscope. TEM measurements were done on a Tecnai F20 microscope from FEI. The samples were dispersed in ethanol and applied onto a carbon-coated copper grid. The chemical composition of the nanocrystals obtained by solvothermal decomposition of precursors in dioctyl ether was examined by in situ TEM–EDX analysis (Tecnai F20 microscope).

4.2. Synthesis of $[Pd(S_2COMe)_2]$ (**1**) and $[Pd(S_2CO^iPr)_2]$ (**2**)

To a solution of $PdCl_2(MeCN)_2$ (0.26 g, 1.00 mmol) in degassed acetonitrile (20 ml) was added a solution of anhydrous NaS_2COMe (0.27 g, 2.07 mmol) in 5 ml acetonitrile. The mixture was stirred at room temperature for half an hour and then filtered through a small Celite pad. The volatiles were removed in vacuo and the residue was recrystallized from dichloromethane–hexane mixture to obtain complex **1** as orange solid. Yield: 0.22g, 85%. Similarly, complex **2** was synthesized as bright yellow-orange solid.

4.3. Syntheses of $[(\eta^3\text{-}CH_2C(CH_3)CR_2)Pd(S_2X)$ (**3**–**6**)

The above procedure was extended to prepare η^3-allylpalladium(II) complexes, **3**–**6** which were obtained by the reaction between chloro-bridged allylpalladium dimers, $[(\eta^3\text{-}CH_2C(CH_3)CR_2)Pd(\mu\text{-}Cl)]_2$ and NaS_2X (X = COMe, COEt, CO^{i}Pr). The characterization data for all the complexes is given below.

4.3.1. Complex **1**

M.p.: 144 (dec). Lit. 145 (dec) [25]. Anal. Calc. for $C_4H_6O_2S_4Pd$: C, 14.97; H, 1.88; S, 39.99. Found: C, 14.85; H, 1.88; S, 39.88%. IR (cm^{-1}): 1252 [ν(C–O)], 1029 [ν(C–S)], 343 [ν(Pd–S)].

4.3.2. Complex **2**

Yield 84% m.p.: 138 °C. Anal. Calc. for $C_8H_{14}O_2S_4Pd$: C, 25.49; H, 3.74; S, 34.03. Found: C, 25.42; H, 3.68; S, 33.98%. IR (cm^{-1}): 1270 [ν(C–O)], 1007 [ν(C–S)], 333 [ν(Pd–S)].

4.3.3. Complex **3**

IR (cm^{-1}): 1243 [ν(C–O)], 1032 [ν(C–S)]. ^1H NMR ($CDCl_3$): δ 1.98 (s, 3H, CH_3 of 2-methylallyl ligand); 2.78 (s, 2H, allyl CH_2); 4.02 (s, 2H, allyl CH_2); 4.20 (s, 3H, CO–CH_3). $^{13}C\{^1H\}$ NMR: δ 23.60 (CH_3 of 2-methylallyl ligand); 58.43 (allyl CH_2); 59.74 (CO–CH_3); 127.26 (C–CH_3); 236.60 (S_2C).

4.3.4. Complex **4**

IR (cm^{-1}): 1242 [ν(C–O)], 1029 [ν(C–S)]. ^1H NMR ($CDCl_3$): δ 1.49 (t, 7 Hz, 3H, OCH_2CH_3); 1.96 (s, 3H, CH_3 of 2-methylallyl ligand); 2.76 (s, 2H, allyl CH_2); 4.03 (s, 2H, allyl CH_2); 4.65 (q, 7.1 Hz, 2H, OCH_2CH_3). $^{13}C\{^1H\}$ NMR: δ 13.91 (OCH_2CH_3); 23.63 (CH_3 of 2-methylallyl ligand); 59.71 (allyl CH_2); 68.64 (OCH_2CH_3); 127.71 (C–CH_3); 235.53 (S_2C).

4.3.5. Complex 5

Yield: 85%. m.p.: 50 °C. Anal. Calc. for $C_8H_{14}OS_2Pd$: C, 32.38; H, 4.75; S, 21.61. Found: C, 32.50; H, 4.30; S, 20.92%. IR (cm^{-1}): 1245 [ν(C–O)]. 1028 [ν(C–S)]. ^1H NMR (C_6D_6): δ 1.02 (d, 6H, COCH(CH_3)$_2$); 1,43 (s, 3H CH_3 of 2-methylallyl ligand); 2.40 (s, 2H, allyl CH_2); 3.61 (s, 2H, allyl CH_2); 5.45 (h, 7 Hz, 1H, COCH(CH_3)$_2$). $^{13}C\{^1H\}$ NMR*: δ 21.61 (COCH(CH_3)$_2$); 23.41 (CH_3 of 2-methylallyl ligand); 59.36 (allyl CH_2); 97.43 (COCH-(CH_3)$_2$); 235.74 (S_2C). * the peak due to C–CH_3 of 2-methylallyl ligand merged in resonances due to solvent C_6D_6.

4.3.6. Complex 6

Yield: 58%. dec. pt. 89–91 °C. $C_8H_{14}OS_2Pd$: C, 32.38; H,4.75; S, 21.61. Found: C, 31.98; H, 4.42; S, 20.75%. IR (cm^{-1}): 1250 [ν(C–O)]. 1030 [ν(C–S)]. ^1H NMR (C_6D_6): δ 1.09 (s, 3H CH_3 allyl); 1.32 (s, 3H, CH_3 allyl); 1.47 (s, 3H, central CH_3); 2.79 (s, 1H, allyl CH_2); 3.15 (s, 1H, allyl CH_2); 3.53 (s, 3H, CO–CH_3). $^{13}C\{^1H\}$ NMR: δ 20.54 (C(CH_3)$_2$); 23.78 (CCH_3); 55.88 (allyl CH_2); 58.13 (S_2COCH_3); 86.97 (C(CH_3)$_2$); 120.34 (C-CH_3); 236.70 (S_2C).

4.4. Synthesis of PdS nanocrystals by bulk thermolysis of complexes 1 and 3

Bulk thermolyses of the complexes, **1** and **3** were performed at 300 °C by heating 0.25 g of each in a quartz boat at a rate of 5 °C min^{-1} from 25 to 300 °C in an atmosphere of dry argon. Once at the required temperature, i.e. 300 °C, an isotherm was maintained for 2 h before allowing the sample to cool to room temperature. The products for both **1** and **3** were dull black materials which formed coarse black shiny powders upon grinding. The typical yields obtained were 74% (**1**) and 85% (**3**), respectively.

4.5. Synthesis of PdS nanocrystals by thermolysis of complexes 3, 4 and 5 in dioctyl ether

The syntheses of PdS nanocrystals were performed using standard air-free techniques. Dioctyl ether (10 ml) was degassed by heating to 100 °C in a vacuum and repeatedly flushing with argon. Subsequently, 0.25 g of the precursors were injected as solutions in dioctyl ether at 100 °C. The temperature was slowly raised to and maintained at 260 °C for 1 h. At the end of reaction, the mixture was cooled to 60 °C, and the nanocrystals were precipitated by adding methanol. The precipitate was isolated by centrifugation.

4.6. Crystal structure determinations

Suitable X-ray quality crystals of complexes **1** and **2** were grown by evaporation from their acetonitrile solutions and for **3** by cooling its THF–hexane solution in freezer for several days and X-ray diffraction studies were undertaken. X-ray crystallographic data were collected from single crystal samples of size, $0.35 \times 0.30 \times 0.30$, $0.21 \times 0.18 \times 0.14$, $0.23 \times 0.18 \times 0.16$ mm^3 for complexes **1**, **2** and **3**, respectively, mounted on a Oxford Diffraction Xcalibur-S CCD system equipped with graphite monochromated Mo Kα radiation (0.71073 Å). The data were collected by ω–2θ scan mode, and absorption correction was applied by using multi-Scan. The structure was solved by direct methods SHELXS-97 and refined by full-matrix least squares against F^2 using SHELXL-97 [37] software. Non-hydrogen atoms were refined with anisotropic thermal parameters. All hydrogen atoms were geometrically fixed and allowed to refine using a riding model.

4.6.1. Crystallographic data for [Pd(S_2COMe)$_2$] (1)

Measurement temperature = 150(2) K, dimensions $0.35 \times 0.30 \times 0.30$ mm, monoclinic, space group $P2_1/c$, $a = 6.2802(3)$ Å, $b = 13.6397(6)$ Å, $c = 10.7961(7)$ Å, $\beta = 97.576(5)°$, $V = 916.72(8)$ Å^3, $Z = 4$, $F(000) = 624$, $d_{calc} = 2.324$ mg/m^3, $\mu = 2.881$ mm^{-1}, 5317 reflections were collected, 1610 unique [$R_{int} = 0.0415$]. Final R indices [$I > 2\sigma(I)$], $R_1 = 0.0487$, $wR_2 = 0.1351$ and $R_1 = 0.0573$, $wR_2 = 0.1492$ (all data) for 102 parameters.

4.6.2. Crystallographic data for [Pd(S_2CO^iPr)$_2$] (2)

Measurement temperature = 150(2) K, dimensions $0.21 \times 0.18 \times 0.14$ mm, monoclinic, space group $P2_1/n$, $a = 9.9319(8)$ Å, $b = 5.8828(5)$ Å, $c = 11.9406(19)$ Å, $\beta = 103.264(11)°$, $V = 679.05(13)$ Å^3, $Z = 4$, $F(000) = 376$, $d_{calc} = 1.843$ mg/m^3, $\mu = 1.960$ mm^{-1}, 3908 reflections were collected, 1189 unique [$R_{int} = 0.0354$]. Final R indices [$I > 2\sigma(I)$], $R_1 = 0.0646$, $wR_2 = 0.1639$ and $R_1 = 0.0789$, $wR_2 = 0.1799$ (all data) for 73 parameters.

4.6.3. Crystallographic data for [(η^3-$CH_2C(CH_3)CH_2$)Pd(S_2COMe)] (3)

Measurement temperature = 120(2) K, dimensions $0.23 \times 0.18 \times 0.16$ mm, triclinic, space group $P\bar{1}$, $a = 4.7707(11)$ Å, $b = 9.530(2)$ Å, $c = 10.727(3)$ Å, $\alpha = 112.68(2)°$, $\beta = 90.51(2)°$, $\gamma = 92.319(18)°$, $V = 449.48(18)$ Å^3, $Z = 2$, $F(000) = 264$, $d_{calc} = 1.985$ mg/m^3, $\mu = 2.461$ mm^{-1}, 4307 reflections were collected, 1579 unique [$R_{int} = 0.0218$]. Final R indices [$I > 2\sigma(I)$], $R_1 = 0.0207$, $wR_2 = 0.0515$ and $R_1 = 0.0249$, $wR_2 = 0.0528$ (all data) for 93 parameters.

Acknowledgements

The authors gratefully acknowledge the help given by Drs. S.K. Gupta and Shovit Bhattacharya in conducting SEM and EDX analyses.

Appendix A. Supplementary material

CCDC 648285, 648286 and 648287 contain the supplementary crystallographic data for **1**, **2** and **3**. These data

can be obtained free of charge via http://www.ccdc.cam.ac.uk/conts/retrieving.html, or from the Cambridge Crystallographic Data Centre, 12 Union Road, Cambridge CB2 1EZ, UK; fax: (+44) 1223-336-033; or e-mail: deposit@ccdc.cam.ac.uk. Supplementary data associated with this article can be found, in the online version, at doi:10.1016/j.jorganchem.2007.08.015.

References

[1] L.Y. Chiang, J.W. Swirczewski, R. Kastrup, C.S. Hsu, R.B. Upasani, J. Am. Chem. Soc. 113 (1991) 6574.
[2] S. Eijsbouts, V.H.J. De Beer, R. Prins, J. Catal. 109 (1988) 217.
[3] M. Misono, N. Nojiri, Appl. Catal. 64 (1990) 1.
[4] J.J. Bladon, A. Lamola, F.W. Lytle, W. Sonnenberg, J.N. Robinson, G. Philipose, J. Electrochem. Soc. 143 (1996) 1206.
[5] C.H. Yang, Y.Y. Wang, C.C. Wan, C.J. Chen, J. Electrochem. Soc. 143 (1996) 3521.
[6] T. Yamamoto, Chem. Abstr. 106 (1987) 8769h.
[7] Y. Idota, M. Yagihara, Chem. Abstr. 106 (1987) 166325s;
Y. Tonomura, J. Handa, Chem. Abstr. 115 (1991) 218921r.
[8] T. Oota, K. Yoshioka, T. Akyama, S. Mori, Chem. Abstr. 123 (1995) 325855j.
[9] A.V. Mashkina, L.G. Sakhaltueva, Kinet. Catal. 43 (2002) 107.
[10] P. Raybaud, J. Hafner, G. Kresse, H. Toulhoat, J. Phys.: Condens. Mat. 9 (1997) 11107.
[11] H. Kyama, T. Iwata, Mitsubishi Paper Mills Ltd., Japanese Patent, 1996, 08/095,209;
O. Tanabe, Fuji Photo Film Co Ltd, US Patent, 1991, 5,030,545.
[12] K. Yamamoto, K. Endo, Y. Takaya and E. Kaneda, Mitsubishi Paper Mills Ltd., Japanese Patent, 1987, 62/226,155.
[13] Y. Tonomura, J. Handa, Mitsubishi Paper Mills Ltd., Japanese Patent, 1991, 03/126,035;
Y. Idota, M. Yagihara, Fuji Photo Film Co Ltd., Japanese Patent, 1986, 61/186,959.
[14] T. Yamamoto, A. Taniguchi, S. Dev, E. Kubota, K. Osakada, K. Kubota, Colloid Polym. Sci. 269 (1991) 969.
[15] M. Schultz, E. Matijevic, Colloids Surf. A 131 (1998) 173.
[16] J. Cheon, D.S. Talaga, J.I. Zink, Chem. Mater. 9 (1997) 1208.
[17] M.A. Malik, P. O'Brien, N. Revaprasadu, J. Mater. Chem. 12 (2002) 92.
[18] A. Birri, B. Harvey, G. Hogarth, E. Subasi, F. Uğur, J. Organomet. Chem. 692 (2007) 2448.
[19] A. Singhal, V.K. Jain, R. Mishra, B. Verghese, J. Mater. Chem. 10 (2000) 1121.
[20] I. Haiduc, Comprehensive Coord. Chem. 1 (2004) 349.
[21] J.O. Hill, J.P. Murray, K.C. Patil, Rev. Inorg. Chem. 14 (1994) 363.
[22] V.G. Bessergenev, E.N. Ivanova, Yu.A. Kovalevskaya, S.A. Gromilov, V.N. Kirichenko, S.M. Zemskova, L.G. Vasilieva, B.M. Ayupov, N.L. Shwarz, Mater. Res. Bull. 30 (1995) 1393.
[23] V.G. Bessergenev, A.V. Bessergenev, E.N. Ivanova, Yu.A. Kovalevskaya, J. Solid State. Chem. 137 (1998) 6.
[24] N. Pradhan, B. Katz, S. Efrima, J. Phys. Chem. B 107 (2003) 13843.
[25] C.G. Sceney, J.O. Hill, R.J. Magee, Thermochim. Acta 6 (1973) 111.
[26] J. Powell, W.-L. Chan, J. Organomet. Chem. 35 (1972) 203.
[27] I. Ara, F. El Bahij, M. Lachkar, N. Ben Larbi, Acta Crystallogr., Sect. C 59 (2003) m199.
[28] G.V. Romanenko, N.V. Podberezskaya, I.A. Baidina, V.V. Bakakin, S.V. Borisov, J. Struct. Chem. 20 (1979) 439.
[29] H.W. Chen, J.P. Fackler Jr., Inorg. Chem. 17 (1978) 22.
[30] K. Nakamoto, Infrared and Raman Spectra of Inorganic and Coordination Compounds, fourth ed., John Wiley & Sons, New York, 1986.
[31] L.F. Dahl, W.E. Oberhansli, Inorg. Chem. 4 (1965) 629;
W.E. Oberhansli, L.F. Dahl, J. Organomet. Chem. 3 (1965) 43.
[32] R. Mason, A.G. Wheeler, J. Chem. Soc. A (1968) 2543;
R. Mason, A.G. Wheeler, J. Chem. Soc. A (1968) 2549.
[33] Joint Committee on Powder Diffraction Standards (JCPDS), 1997, Card No. 25-1234.
[34] "POWDERX" – A program for indexing and refinement of X-ray data written by Dr. V.K. Wadhavan, Bhabha Atomic research Centre, private communication.
[35] Y. Zhang, Z. Yuan, R.J. Puddephatt, Chem. Mater. 10 (1998) 2293.
[36] A.I. Vogel, Practical Organic Chemistry, third ed., Longman, London, 1966, p. 499.
[37] G.M. Sheldrick, SHELX-97 – A Program for Crystal Structure Solution and Refinement, University of Gottingen, Germany, 1997.